Entrainment to the CIECAM02 and CIELAB colour appearance models in the human cortex

Andrew Thwaites[1,2]*, Cai Wingfield[1,3], Eric Wieser[4], Andrew Soltan[5], William D. Marslen-Wilson[1,2], Ian Nimmo-Smith[2]

[1] Department of Psychology, University of Cambridge, Cambridge, UK

[2] MRC Cognition and Brain Sciences Unit, Cambridge, UK

[3] Department of Psychology, University of Lancaster, Lancaster, UK

[4] Department of Engineering, University of Cambridge, Cambridge, UK

[5] School of Clinical Medicine, University of Cambridge, Cambridge, UK

*Corresponding author. Department of Psychology, Downing Site, University of Cambridge, Cambridge, CB2 3EB, United Kingdom

E-mail address: acgt2@cam.ac.uk

32 *Abbreviations:* V1, primary visual cortex; EMEG, electro- and magneto-
33 encephalographic; KID, Kymata identifier; CIECAM02, the CIE (2002) colour
34 appearance model; CIELAB, the CIEL*A*B (1976) colour space; ERG,
35 electroretinographic; LGN, lateral geniculate nucleus
36

Abstract

In human visual processing, information from the visual field passes through numerous transformations before perceptual attributes such as colour are derived. The sequence of transforms involved in constructing perceptions of colour can be approximated by colour appearance models such as the CIE (2002) Colour Appearance Model, abbreviated as CIECAM02. In this study, we test the plausibility of CIECAM02 as a model of colour processing by looking for evidence of its cortical entrainment. The CIECAM02 model predicts that colour is split into two opposing chromatic components, red-green and cyan-yellow (termed CIECAM02-a and CIECAM02-b respectively), and an achromatic component (termed CIECAM02-A). Entrainment of cortical activity to the outputs of these components was estimated using measurements of electro- and magnetoencephalographic (EMEG) activity, recorded while healthy subjects watched videos of dots changing colour. We find entrainment to chromatic component CIECAM02-a at approximately 35 ms latency bilaterally in occipital lobe regions, and entrainment to achromatic component CIECAM02-A at approximately 75 ms latency, also bilaterally in occipital regions. For comparison, transforms from a less physiologically plausible model (CIELAB) were also tested, with no significant entrainment found.

(180 words)

1 Introduction

As information travels through the human visual system, it is subjected to a variety of transformations. First, the cornea and the lens alter the spectral content of incoming light (Bone and Sparrock, 1971). This filtered light then strikes the retina, where photoreceptor cones with different spectral absorption rates activate at different wavelengths (Stockman et al., 1999; Stockman and Sharpe, 2000). The excitation from these photoreceptors (L-, M- and S-cones) is integrated through sets of neuronal cells in the inner retinal layer, which quantifies the colour information into three opponent channels. The first of these channels quantifies achromatic information[1], and is comprised of the aggregate L and M excitation information (sometimes written 'L+M')[2]. The remaining two channels quantify chromatic information: the 'L-M' cone opponent channel (comprised of the difference between the incoming L and M signals) is the basis of the red-green channel of colour vision, while 'S-[L+M]' (in which the S-cone signals are antagonistic to those from L- and M-cones) is the basis of the cyan-yellow channel (Lee and Silveira, 2016). Each channel projects from the retina into the lateral geniculate nucleus (LGN); the L+M channel projecting predominantly to the magnocellular layer; the L-M channel to the parvocellular layer, and the S-[L+M] channel to the koniocellular layer. These channels are thus also known as the MC-, PC- and KC-pathways. From the LGN, the pathways project into an area of the visual cortex known as V1, where colour information is passed to the extra striate cortex. The precise nature of the transformations involved in the processing of colour from V1 onwards is less clear (Conway, Chatterjee, et al., 2010; Shapley and Hawken, 2011; Johnson and Mullen, 2016).

One of the most effective ways to ascertain the sequence of transformations that visual information undergoes has been to examine whether hypothesised transformations are 'tracked' by neuronal or cortical activity, a phenomenon known as entrainment (Ding, et al., 2014; Ding and Simon, 2014). For example, the L+M and L-M transformations are found to be entrained in both electroretinogram (ERG) and intracellular in vitro recordings on inner retinal layers (ERG: Kremers and Link, 2008; Kremers et al, 2010; Parry et al, 2012; see Kremers et al (2016) for overview; intracellular recordings: Dacey et al, 1996).

The ability to model sequences of transformations is therefore an important precursor to testing for evidence of entrainment. While the transformations that have taken place at the retina are relatively straightforward (with visual information having passed through a relatively small number of neurons), hypothesising the sequence of transformations at V1 or beyond is more challenging. The most comprehensive of these later sequences are the 'colour appearance' models, which characterise the transformations hypothesised to occur in the perception of colour. The formulation of

---

[1] The achromatic response is sometimes referred to as 'luminance'.
[2] The extent to which S-cone information contributes to the achromatic channel is a question of some debate (Ripamonti et al, 2009).

94 these models has historically been informed both by retinal physiology and the
95 behavioural responses of human observers to colour stimuli (Luo and Hunt 1998).

96 In the current study, we test four hypothesised transformations for cortical
97 entrainment, comprising the achromatic and red-green transformations from each of
98 two colour appearance models, CIELAB and CIECAM02. CIELAB was developed
99 during the 1970s and served for many years as the Joint ISO/CIE Standard for colour
100 appearance; its successor, CIECAM02, was released in 2002 and included the
101 addition of more complex features which aimed to model the visual system and
102 observed behavioural responses to colour perception more accurately (Moroney et al.,
103 2002). While the use of CIELAB is prevalent, being widely used in the domains of
104 technology and engineering, it is less physiologically plausible than its successor, and
105 can be considered a naïve baseline model against which CIECAM02 can be
106 compared. The CIECAM02 achromatic transformation is referred to as CIECAM02-
107 A, while the red-green chromatic transformation is referred to as CIECAM02-a. Their
108 CIELAB counterparts are denoted CIELAB-L and CIELAB-A respectively.

109 As noted by Parry et al. (2012), both achromaticity and chromaticity are known to be
110 computed in parallel, and as a result it is possible to observe entrainment of the two
111 transformations simultaneously using a single stimulus. In the current study, we use
112 an established procedure (Thwaites et al., 2015; 2016; 2017) to search for evidence of
113 entrainment to CIECAM02 and CIELAB in the neural activity of regions of the cortex
114 (striate, extra striate, and regions beyond), measured by electroencephalography
115 (EEG) and magnetoencephalography (MEG). Specifically, we aim to determine (1)
116 whether entrainment to achromaticity and chromaticity occurs for either model, and if
117 so: (2) the latencies and (3) location of this entrainment.

118 Evidence of entrainment of both achromatic and red-green colour opponency has
119 already been identified in the visual-occipital cortex. EEG and MEG studies have
120 identified entrainment directly (achromatic: Regan, 1966; Herrmann, 2001;
121 chromatic: Cheng et al., 2001; Nishifuji et al., 2006) and when the signal has been
122 convolved with an impulse response, estimated using evoked spread spectrum
123 analysis (Lalor et al., 2006, VanRullen and Macdonald, 2012). Evidence of
124 entrainment of achromatic and red-green colour opponency to blood oxygenation
125 levels (BOLD), measured through functional Magnetic Resonance Imaging (fMRI),
126 has also been reported (achromaticity: Kwong, et al (1992); Ogawa et al., 1992;
127 Wandell and Winawer, 2011 for historical overview; red-green response: McKeefry
128 and Zeki (1997), Hadjikhani et al., 1998). The current study is first to test for
129 evidence of entrainment to the widely adopted specific colour appearance models
130 CIECAM02 and CIELAB, as well as being the first reporting precise latencies of that
131 entrainment.

132 In addition to the static graphic presentation of results in this paper, a dynamic,
133 interactive representation of this study's results can be viewed on the online Kymata

134 Atlas (http://kymata.org). For easy reference, each hypothesised transformation in this
135 paper (referred to as a 'function' in Kymata) is assigned a *Kymata ID* (KID).

136

2 Methods

2.1 Defining candidate models

139 A suitable model is one that takes a set of time-varying signals as input (in this case
140 the visual field) and produces a time-varying signal as output (the predication of
141 neural activity). The model must be characterized by a function *f*, taking the form:

142 $$f(x_1, x_2, x_3, ..., x_t) = (y_1, y_2, y_3, ..., y_t), \qquad \text{(eq 1)}$$

143 where input $(x_1, ..., x_t)$ and output $(y_1, ..., y_t)$ are both time-courses of length *t*, and
144 where *f* is bounded by a set of formal requirements (Davis et al., 1994) and the
145 additional requirement that y_i cannot be dependent on any x_k where $k > i$. This latter
146 requirement excludes non-causal functions from the outset, such that each output y_i
147 can depend only on the input history $(x_1, ..., x_i)$. In the current work, we test models
148 that are a special case, where y_i is dependent on x_i alone (although we consider the
149 opportunity for testing models that make use of historical inputs in the discussion).
150
151 In the following section, we specify four candidate models based on different
152 hypothesised transforms of visual data.

153

2.2 The CIECAM02 models

155
156 Colour appearance models seek to capture the perception of colour under diverse
157 viewing conditions (Fairchild, 2013). The foundation of these models lies in colour
158 opponency (Hering, 1878), in which there are two opposing colour dimensions: red-
159 green and cyan-yellow. Together with an achromatic response value, these allow the
160 full range of colours to be encoded (see Judd, 1951; Wandell, 1995 for overview).

161 In this study we consider a contemporary colour appearance model based on opponent
162 colour, the CIE (2002) Colour Appearance Model (Moroney et al., 2002), abbreviated
163 as CIECAM02. A simplified schematic is shown in Fig 1C. First, the stimulus colour
164 is represented as L(*t*), M(*t*), S(*t*) tristimulus values, in the LMS-space of Li et al.
165 (2002). These are then transformed to the L´M´S´-space (Hunt-Pointer-Estevez space)
166 of Hunt and Pointer (1985)[3]:

---

[3] LMS- and L´M´S´-space are also referred to as RGB- and R´G´B´-space by some
authors, including Moroney et al., Li et al., and Hunt and Pointer.

167 $$\boldsymbol{L'M'S'}(t) = \begin{bmatrix} L'(t) \\ M'(t) \\ S'(t) \end{bmatrix} = \begin{bmatrix} 0.38971 & 0.68898 & -0.07868 \\ -0.22981 & 1.18340 & 0.04641 \\ 0.00000 & 0.00000 & 1.00000 \end{bmatrix} * \begin{bmatrix} L(t) \\ M(t) \\ S(t) \end{bmatrix} \quad \text{(eq. 2)}$$

168 where $L(t)$, $M(t)$, and $S(t)$ are the viewing-condition-adapted tristimulus values in
169 LMS-space of the stimulus at time t.

170 These L´, M´ and S´ values then undergo non-linear response compression based on a
171 generalised Michaelis-Menten equation:

172

173 $$L'_a(t) = \frac{400(F_L L'(t)/100)^{0.42}}{27.13 + (F_L L'(t)/100)^{0.42}} + 0.1 \qquad \text{(eq. 3)}$$

174

175 where F_L is a luminance-level adaptation factor specific to the viewing parameters
176 (see Fairchild (2013) for discussion). Values of $M'_a(t)$ and $S'_a(t)$ can be calculated
177 from $M'(t)$ and $S'(t)$ in a similar manner, substituting L' with M' or S'.

178 The complete pipeline of transforms for CIECAM02, and their justifications, can be
179 found in Moroney et al.'s CIECAM02 schema.
180
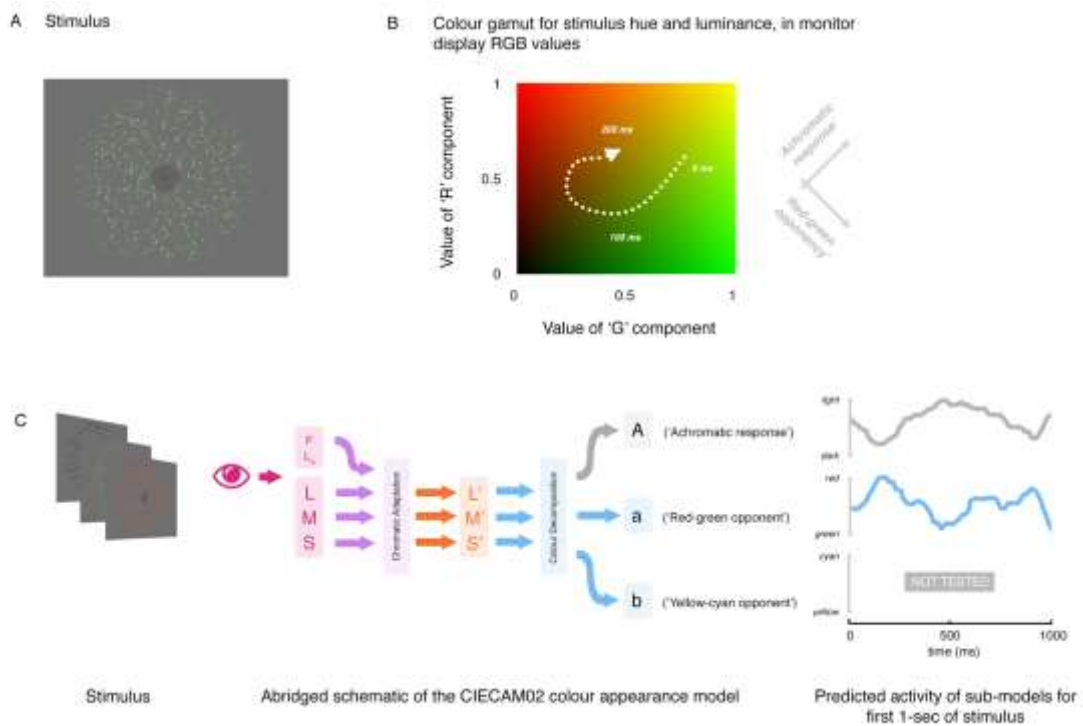
182 **Fig 1. Example of the stimulus, and model predictions.** A. The stimulus consisted of coloured dots
183 on a grey background, with a fixation cross in the centre. B. The colour of the dots varied over time,
184 and was generated by taking a random trajectory through a red-green-black-yellow colour gamut. C.
185 Abridged schematic of the CIECAM02 colour appearance model, together with the predicted
186 electrophysiological activation of the *achromatic response* (CIECAM02-A) and *red-green*
187 (CIECAM02-a) model components for the first second of the stimulus.

188

2.2.1 CIECAM02-A (KID: Q5D5M)

The function CIECAM02-A models the achromatic response to a stimulus in the visual field. It takes the form:

$$CIECAM02\_A(t) = [2L_a(t) + M'_a(t) + (1/20)S'_a(t) - 0.305]N_{bb} \qquad (eq.\ 4)$$

where L'_a(t), M'_a(t), and S'_a(t) are the compressed L'(t), M'(t) and S'(t) values of the stimulus at time t and N_{bb} is the chromatic induction factor specific to the viewing condition parameters. The value of this variable over the first 1 second of the stimulus is shown in Fig 1C.

197

2.2.2 CIECAM02-a (KID: URKWX)

The function CIECAM02-A models the red-green colour opponent value of a stimulus in the visual field. It takes the form:

$$CIECAM02\_a(t) = 2L'_a(t) - 12M'_a(t)/11 + S'_a(t)/11 \qquad (eq.\ 5)$$

where L'_a(t), M'_a(t), and S'_a(t) are the compressed L'(t), M'(t) and S'(t) values of the stimulus at time t. The value of this variable over the first 1 second of the stimulus is shown in Fig 1C.

205

2.3 The CIELAB models

The CIELAB colour appearance model (also known as CIEL*A*B*) is a precursor to CIECAM02. Like CIECAM02, it models colour opponency, but is comparatively naïve and ignores physiologically plausible features of colour processing such as the application of chromatic adaptation to a space closer to cone fundamental space (Fairchild, 2013). Despite its relative simplicity, CIELAB is a widely used colour space employed in cameras and visual processing equipment, and was adopted as a Joint ISO/CIE Standard (ISO 11664-4:2008(E)/CIE S 014-4/E:2007). In this study we use it as a naïve comparator to the more physiologically plausible CIECAM02.

215

2.3.1 CIELAB-L (KID: 68RA6)

The function CIELAB-L models the achromatic response to a stimulus in the visual field. Its inputs are X(t), Y(t), and Z(t) tristimulus values, defined in the CIE 1931 XYZ colour space (ISO 11664-1:2007). The model takes the following form:

220
221

$$CIELAB\_L(t) = 116\left(\begin{cases} if\ Y(t)/Y_{ref}(t) > 0.008856\ then\ \left(Y(t)/Y_{ref}(t)\right)^{1/3} \\ else\ 7.787 * \left(Y(t)/Y_{ref}(t)\right) + 16/116 \end{cases}\right)$$

where Y(t) is the average tristimulus value over the visual field, and Y_{ref}(t) is the
normalised tristimulus value of the reference field (in this experiment Y_{ref}(t) was kept
constant at a value of 100).

2.3.1 CIELAB-A (KID: UYBPJ)

The function CIELAB-A models the red-green colour opponent value of a stimulus in
the visual field. It takes the following form:

$$CIELAB\_A(t) = 500\left(\begin{cases} if\ X(t)/X_{ref}(t) > 0.008856\ then\ \left(X(t)/X_{ref}(t)\right)^{1/3} \\ else\ 7.787 * \left(X(t)/X_{ref}(t)\right) + 16/116 \end{cases}\right.$$

$$\left. -\begin{cases} if\ Y(t)/Y_{ref(t)} > 0.008856\ then\ \left(Y(t)/Y_{ref(t)}\right)^{1/3} \\ else\ 7.787 * \left(Y(t)/Y_{ref(t)}\right) + 16/116 \end{cases}\right)$$

where X(t) and Y(t) are the average tristimulus values of the visual field, and X_{ref}(t)
and Y_{ref}(t) are the tristimulus values of the reference field (in this experiment we used
constant values X_{ref}(t) = 95.04 and Y_{ref}(t) = 100).

2.4. The analysis procedure

The reconstructed distributed source current of the cortex is specified as the current of
10,242 cortical regions (sources), spaced uniformly over the cortex. The testing
procedure involves examining each of these sources, looking for evidence that the
current predicted by a model is similar to the current observed (Fig. 2A). This
procedure is repeated at 5 ms intervals (Fig. 2B) across a range of time-lags ($-200 < 1$
< 800 ms), covering the range of plausible latencies (0 to 800 ms) and a short, pre-
stimulation range (-200 to 0 ms) during which we expect to see no entrainment. This
produces a statistical parametric map that changes over time as the lag is varied,
revealing the changes in similarity of a given model's predicted behaviour with
observed behaviour over the cortical surface. Evidence of a model's similarity
between its predicated behaviour and measured cortical activity is expressed as a p-
value, which is generated through the match-mismatch technique described in
Thwaites et al. (2015), where evidence for similarity is described as significant if the
p-value falls below a pre-defined threshold, α*. We refer to the observation of
significant matches at a specific lag and location as 'model expression'.

258

259
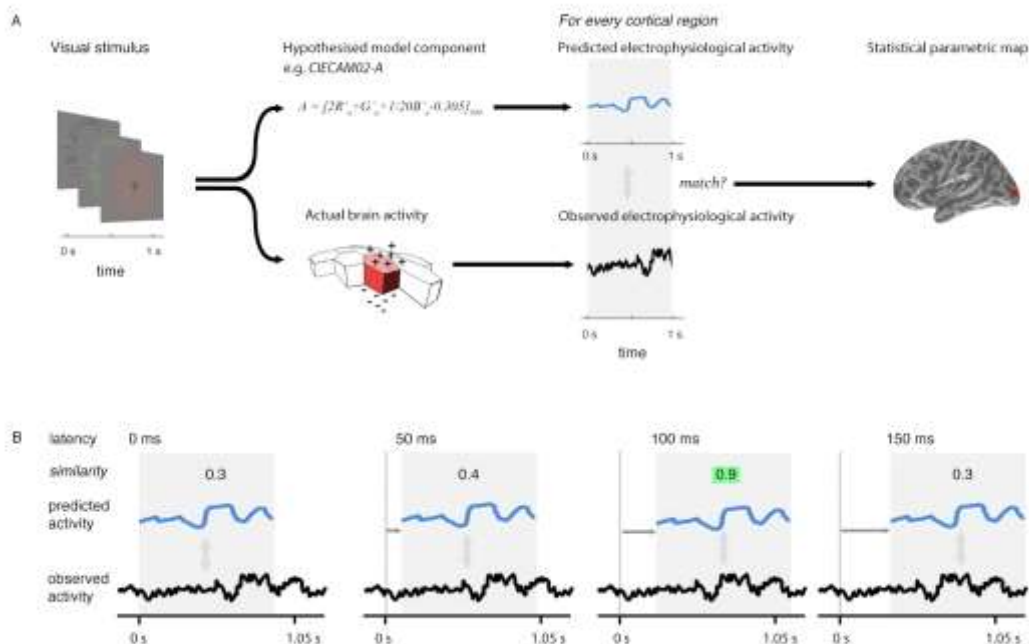
Fig 2. Technique overview. First (A), the electrophysiological activity of the brain in response to a given stimulus (measured using EMEG) is matched to the pattern of neural activity predicted by the model being evaluated. Predicted and observed activity are tested for similarity and the resulting Statistical Parametric Map (SPM) displays the regions (vertices) where the match is statistically significant. Second (B), this procedure is repeated at different lags (illustrated here from 0-150 ms) between the onset of the observed neural activity and the onset of the predicted output. We record the lag at which the similarity is greatest (highlighted). This produces an SPM that changes over time.

Setting α^* so that it accurately reflects what we know about the data being tested can be difficult. In the current study, some of the measurements used in the tests would be dependent on other measurements (because of spatial and temporal similarities between neighbouring sources and lags). However, it is very difficult, if not impossible, to get accurate estimations of, for instance, the spatial dependencies between sources. In the present study, rather than accept assumptions about the dependencies that are hard to justify, we assumed that the data at each source and lag were independent (a 'worst case' scenario), prompting us to use a Bonferroni-type correction. As a result, the reader should be aware that the type II error rate is likely to be high, making the reported results very conservative.

We used the formula for the familywise false alarm rate from Thwaites et al. (2015) to generate an α^* of approximately 3×10^{-13}; p-values greater than this are deemed to be not significant.

The results are presented as *expression plots*, which show the latency at which each of the 10,242 sources per hemisphere best matched the output of the tested model

283 (marked as a 'stem'). On the y-axis is the evidence of the match at this latency: if any
284 of the sources have evidence, at their best latency, indicated by a p-value lower than
285 α*, they are deemed significant matches and the stems are coloured red, blue, pink
286 and green depending on the model.

287 The expression plots also allow us to chart which models are most likely to be
288 entrained at a particular source through a model selection procedure, using p-values as
289 a proxy for model likelihood. By default, the expression plot displays only the best
290 model (i.e. the one with the lowest p-value) for a source. It is important to note that
291 this model selection procedure does not indicate that any one model is *significantly*
292 better than another for some source. It indicates only that one model fits the data to a
293 somewhat higher degree than another, even if this evidence may not differ strongly
294 between models. We take this approach as we are only interested in the trend of
295 which models explain the activity best in each source, and to disambiguate between
296 models which may be correlated over time.

297

2.5.   MEG and EEG Methods and Materials

2.5.1   Experiment design

300 *Participants:* 15 right-handed participants (7 men, mean age = 24 years, range=18-30)
301 were recruited. All gave informed consent and were paid for their participation. The
302 study was approved by the Peterborough and Fenland Ethical Committee (UK), and
303 the study was carried out in accordance with the Code of Ethics of the World Medical
304 Association (Declaration of Helsinki).
305
306 *Stimuli*: A pattern of randomly placed dots with a grey mask in the surrounds and
307 centre. The centre also contained a black fixation cross (Fig. 1A). The colour and
308 horizontal movement of these dots fluctuated pseudo-randomly. The stimulus lasted 6
309 minutes and 40 seconds, allowing it to be split later in the analysis procedure into 400
310 segments of length 1000 ms. 10 seconds of stimulus were added to the beginning and
311 end of the stimulus to avoid the sudden appearance and disappearance of the stimulus
312 during the first and last trial.

313 The colour of the dots during the experiment was controlled by independently
314 fluctuating the R and G base components of the monitor display pixels between 0.3
315 and 1. The B base component remained at zero throughout the experiment. Although
316 values for the monitors R and G were explicitly manipulated, the axes of interest are
317 at roughly 45 degrees to this: the red-green opponency dimension (i.e., the ratio of red
318 to green in the colour's hue), and achromaticity dimension (the luminance of the
319 resulting colour value). These fluctuations were pseudo-periodic, with frequencies
320 ranging between 4 and 40Hz (see Fig 1B).

321 Although the B base component remained constant during the stimulus, it does not
322 follow that the cyan-yellow opponency response (not tested during the study) likewise

323 remained constant. Indeed, this would not be possible without choosing a measure of
324 cyan-yellow opponency beforehand: CIECAM02 and CIELAB define the cyan-
325 yellow chromaticity dimensions in different manners, and they cannot both be
326 maintained at a single value simultaneously. Thus, the choice to fix $B = 0$ was made
327 to simplify the stimulus definition and not to control for the B-component in the
328 signal.

329

2.5.2. Procedure

331 Each participant received one practice stimulus lasting 20 seconds. The continuous 6
332 minute and 40 second stimulus was played 4 times to the participant, with instructions
333 to fixate on the cross in the middle of the screen. After each presentation, the
334 participant could rest, playing the next presentation when ready, using a button box.
335 Presentation of stimuli was controlled with Matlab, using the Psychophysics Toolbox
336 extensions (Brainard, 1997; Pelli, 1997; Kleiner et al., 2007). The stimuli were
337 presented on a Panasonic PT-D7700 DLP projector, with the central wavelengths of
338 the red, green and blue base components being 610, 550 and 472 nm respectively
339 (measured using a Coherent Inc. spectroscope), while the CIE xyY coordinates of
340 these components were (0.64, 0.33, 0.22), (0.26, 0.61, 0.71) and (0.16, 0.07, 0.72)
341 respectively (measured using an Admesy Brontes tristimulus colorimeter). The
342 energies of these components were Gamma-corrected for the projector.

343 To keep participants alert during the experiment, the subjects listened passively to an
344 audio podcast (a BBC radio talk-show) while watching the stimuli.

345

2.5.3 Modelling the predicted CIECAM02 and CIELAB entrainment responses

347 The changing hue and luminance of the colours were displayed on the projector in
348 monitor RGB format (as described in section 2.5.1). However, the CIECAM02 and
349 CIELAB models both require the momentary XYZ tristimulus values (and their
350 accompanying viewing parameters) as input. An Admesy Brontes tristimulus
351 colorimeter was used to measure the momentary XYZ values of the projector stimulus
352 over time, giving an accurate measurement of these values during the projection of
353 the stimulus. These XYZ values (together with measurement or estimation of the
354 accompanying viewing parameters), were then used to calculate the CIELAB and
355 CIECAM02 responses, using the equations given in section 2.2 and 2.3.

356

2.5.4. EMEG recording

358 Continuous MEG data were recorded using a 306 channel VectorView system
359 (Elekta-Neuromag, Helsinki, Finland) containing 102 identical sensor triplets (two
360 orthogonal planar gradiometers and one magnetometer) in a hemispherical array

situated in a light magnetically-shielded room. The position of the head relative to the sensor array was monitored continuously by four Head-Position Indicator (HPI) coils attached to the scalp. Simultaneous EEG was recorded from 70 Ag-AgCl electrodes placed in an elastic cap (EASYCAP GmbH, Herrsching-Breitbrunn, Germany) according to the 10/20 system, using a nose electrode as reference. Vertical and horizontal EOG were also recorded. All data were sampled at 1 kHz with a band-pass filter from 0.03-330 Hz. A 3-D digitizer (Fastrak Polhemus Inc., Colchester, VA) recorded the locations of the EEG electrodes, the HPI coils and approximately 50-100 'headpoints' along the scalp, relative to three anatomical fiducials (the nasion and left and right pre-auricular points).

2.5.5. Data pre-processing

Static MEG bad channels were detected and excluded from subsequent analyses (MaxFilter version 2, Elekta-Neuromag, Stockholm, Sweden). Compensation for head movements (measured by HPI coils every 200 ms) and a temporal extension of the signal–space separation technique (Taulu et al., 2005) were applied to the MEG data. Static EEG bad channels were visually detected and removed from the analysis (MNE version 2.7., Martinos Center for Biomedical Imaging, Boston, Massachusetts). The EEG data were re-referenced to the average over all channels. The continuous data were low-pass filtered to 100 Hz (zero-phase shift, overlap-add, FIR filtering). The recording was split into 400 epochs of 1000 ms duration. Each epoch included the 200 ms from before the epoch onset and 800 ms after the epoch finished (taken from the epoch previous and subsequent) to allow for the testing of different latencies. Epochs in which the EEG or EOG exceeded 200 µV, or in which the value on any gradiometer channel exceeded 2000 fT/m, were rejected from both EEG and MEG datasets (between 5% and 15%, depending on the participant). Epochs that were not rejected were averaged over all four stimulus repetitions.

2.5.6. Source Reconstruction

The location of the cortical current sources was estimated using minimum-norm estimation (MNE; Hämäläinen and Ilmoniemi, 1994), neuro-anatomically constrained by MRI images obtained using a GRAPPA 3D MPRAGE sequence (TR=2250 ms; TE=2.99 ms; flip-angle=9 degrees; acceleration factor=2) on a 3T Tim Trio (Siemens, Erlangen, Germany) with 1 mm isotropic voxels. For each participant a representation of their cerebral cortex was constructed using FreeSurfer (Freesurfer 5.3, Martinos Center for Biomedical Imaging, Boston, Massachusetts) from their individual MR images. The forward model was calculated with a three-layer Boundary Element Model using the outer surface of the scalp and the outer and inner surfaces of the skull identified in the structural MRI. Anatomically-constrained source activation reconstructions at the cortical surface were created by combining MRI, MEG, and

401 EEG data. The MNE representations were down-sampled to 10,242 vertices per
402 hemisphere, roughly 3mm apart, to improve computational efficiency.
403 Representations of individual subjects were aligned using a spherical morphing
404 technique (Fischl et al., 1999). Source activations for each trial were averaged over
405 participants. We employed a loose-orientation constraint (0.2) to improve the spatial
406 accuracy of localization. Sensitivity to neural sources was improved by calculating a
407 noise covariance matrix based on a 1 second pre-stimulus period. Reflecting the
408 reduced sensitivity of MEG sensors for deeper cortical activity (Hauk et al., 2011),
409 sources located on the cortical medial wall and in subcortical regions were not
410 included in the analyses reported here.

411 The entrainment testing procedure (section 2.4) was performed on these participant-
412 average source reconstructions.

413

2.5.7. Visualization

415 The cortical slices in Fig 3. use the visualization software MRIcron (Georgia State
416 Center for Advanced Brain Imaging, Atlanta, Georgia) with results mapped to the
417 high-resolution colin27 brain (Schmahmann et al., 2000).

418

3. Results

3.1 CIECAM02 model

3.1.1 CIECAM02-A component ('the achromatic response')

422 The regions where expression for the CIECAM02-A model was the most significant
423 of the models tested — and below the α^* threshold — were located bilaterally at 75
424 ms (Fig. 3B), centred in regions in the occipital lobe. An interactive representation of
425 this model (and all models tested in this paper) can be viewed using the Kymata Atlas
426 (2016).

427
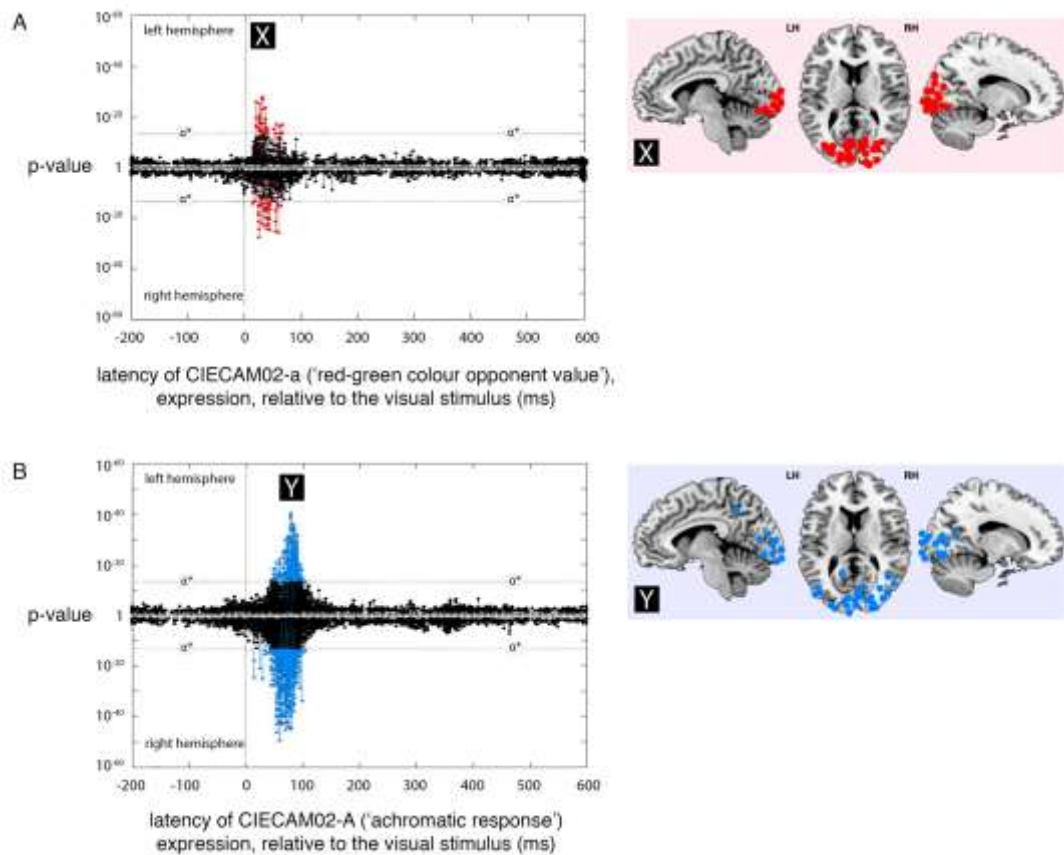
**Fig 3. Expression plots for CIECAMO2-A and CIECAMO2-a from the CIECAM02
colour appearance model. A)** Plot for the expression for the CIECAMO2-a model across
processing lags from -200 to +600 ms, relative to the visual environment. Results for the left
and right hemispheres are plotted separately, mirror-wise across the mid-line. The minimum
p-values at a given source, over all latencies, are marked as 'stems'. Stems at or 'above' the
stipulated value ($p \simeq 3{\times}10^{-13}$) indicate significant expression of the CIECAMO2-a (red) at
that source. **B)** Plot for the expression for the CIECAMO2-A model (blue). The peaks for
both models' significant expression are marked X (at 35 ms, CIECAMO2-a) and Y (75 ms,
CIECAMO2-A). The cortical locations of significant sources are indicated on the coronal and
sagittal slices to right of the plots. These plot implements model selection (see **section 2.4**) so
that each source only appears once in 3A, 3B, 4A and 4B.

439

440   The locations (namely ventral, posterior parietal, calcarine sulcus and occipital lobe
441   regions) are approximate in all cases, as a consequence of the error introduced by the
442   point-spread function inherent in EMEG source localization (see discussion). This
443   spatial ambiguity means it is not possible to narrow these locations to specific visual
444   areas, beyond noting that the entrainment is centred around the occipital pole (V1).

445

446   **3.1.2 CIECAM02-a component ('red-green opponent colour dimension')**

15

447 The regions where expression for the CIECAM02-a model was the most significant of
448 the two models tested, and passed the α* threshold, were located bilaterally at 35 ms
449 (Fig. 3A). Like CIECAM02-A, these regions were centred in ventral, posterior
450 parietal, calcarine sulcus and occipital lobe.

451

452 **3.1.2 CIELAB-L and CIELAB-a components**

453 No significant expression was found for either CIELAB-L or CIELAB-A, at any
454 latency (Fig. 4).
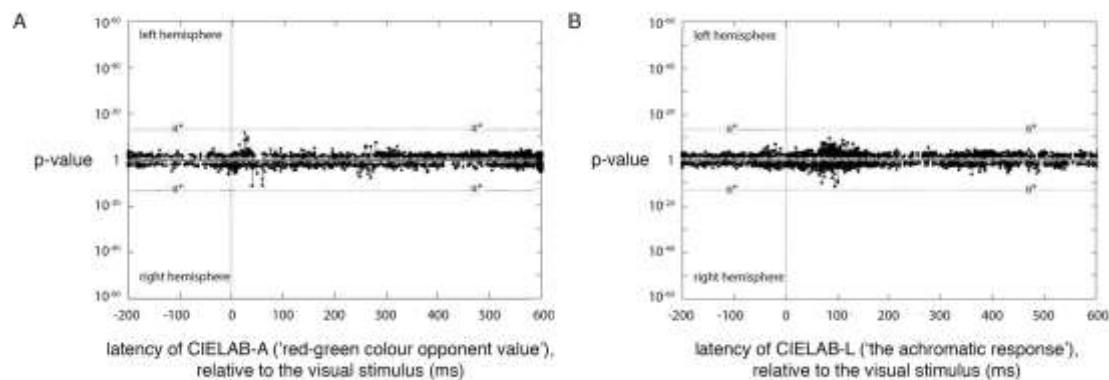
455

456 **Fig 4. Expression plots for CIELAB-A and CIELAB-L from the CIELAB colour**
457 **appearance model. A)** Plot for the expression for the CIELAB-A across lags from -200 to
458 +600 ms, relative to the visual environment. **B)** Plot for the expression for the CIELAB-L.
459 Neither show significant entrainment at any latency.
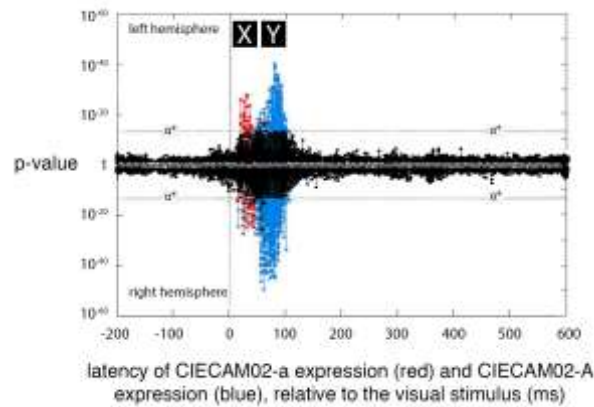
460

461 **4 Discussion**

462 As noted in the introduction, entrainment to the transformations for both
463 achromaticity and red-green opponency are found in the output of the inner retinal
464 layer as inputs to the MC- and PC-pathway respectively. The question in this study
465 was whether entrainment to CIECAM02 models of these features can be found in the
466 cortical activity at the point where these pathways enter the cortex. Our results
467 indicate that this is the case: evidence of significant entrainment for both CIECAM02-
468 A and CIECAM02-a is centred bilaterally in the polar occipital cortex, the region of
469 visual area V1, and the region where the afferent pathways project into the cortex.
470 Although focused on the poles, there is significant entrainment of the output for both
471 transformations in ventral, posterior parietal, and calcarine sulcus areas. The reader
472 should be cautious about narrowing down the location of the entrainment to either
473 component more narrowly. The inherent insolvability of the inverse problem during
474 EMEG source reconstruction (Grave de Peralta-Menendez et al., 1996; Grave de
475 Peralta-Menendez and Gonzalez-Andino, 1998) means that substantial 'point spread'
476 of localization data may be present. Improvements in source reconstruction (through

477   the gathering of more data or improved inverse techniques) may reduce this error in
478   the future.

479   These findings are consistent with previous reports which locate entrainment to
480   chromaticity and achromaticity in the human visual-occipital cortex, in both dendritic
481   current (Regan, 1966; Herrmann, 2001; Cheng et al., 2001; Nishifuji et al., 2006) and
482   blood oxygenation levels (Kwong, et al (1992); Ogawa et al., 1992; McKeefry and
483   Zeki (1997), Hadjikhani et al., 1998). However, the current study is the first to test for
484   evidence of entrainment to CIECAM02 and CIELAB. Historically, the most
485   informative entrainment studies have been those in which the outputs of explicit
486   physiological mechanisms (modelled as mathematical transforms) are tested: a
487   preeminent example is Derrington and colleagues, who, in their landmark study
488   (Derrington et al, 1984), tested the entrainment of cell responses in the PC- and MC-
489   pathway to the modulation of opponency channels modelled on the physiologically-
490   based 'MBDKL' colour space (MacLeod and Boynton, 1978; Derrington et al, 1984).
491   This ability to link the predictions of such models with measured physiological
492   responses is a powerful tool in assessing the plausibility of the model themselves. The
493   current study, which tests the plausibility of two rival models that aim to characterise
494   both perceptual and physiological properties (CIECAM02, and CIELAB) against each
495   other, emphasises this potential: the results demonstrate significant entrainment to
496   CIECAM02 achromaticity and red-green opponency (Fig 3), compared with no
497   significance for their CIELAB counterparts (Fig 4). The insignificance of CIELAB is
498   no doubt due to the fact that, compared with CIECAM02, it is comparatively naïve;
499   CIELAB ignores physiologically plausible features of colour processing such as
500   chromatic adaptation to a space akin to that of the cone fundamentals, features which
501   are modelled by CIECAM02. As a result, the entrainment pattern of CIECAM02 is
502   likely to match the observed electrophysiological activity better than that of that of
503   CIELAB, leading to the analysis procedure giving the former a higher plausibility.

504   The most striking difference between the CIECAM02 achromatic and red-green
505   response components is the latency difference: CIECAM02-a is entrained at 35 ms,
506   while CIECAM02-A is entrained at 75ms, a full 40 ms later (Fig 3; Fig 5). This result
507   is consistent with previous findings showing the achromatic response lagging the
508   chromatic response (e.g. Walraven and Leebeek, 1964, see Kommanapalli et al (2014)
509   for overview). Kommanapalli et al. (2014) argue that this difference may be due to
510   retinal physiology: L- and M- cones that serve as inputs to chromatic (parvocellular)
511   ganglion cells appear to provide their respective inputs at the same latency (Smith et
512   al, 1992); by contrast, L- and M- cones inputs to achromatic (magnocellular) ganglion
513   cells appear to provide their respective inputs at different latencies (with M- lagging
514   L- between 5 and 35 ms), and it is plausible that this delay of the M- input relative to
515   the L- input results in the entire achromatic pathway being delayed with respect to its
516   chromatic counterpart. It is worth noting that a delay of achromatic information
517   relative to chromatic information does not contradict evidence that red-green colour
518   opponency responses appear to be lost at high temporal frequencies (Ives, 1912), a

519 result that has traditionally been taken as evidence that the MC-pathway is able to
520 process achromatic signals 'more rapidly' than the red-green PC-pathway. The fact the
521 achromatic pathway is able to encode higher frequencies than the red-green pathway
522 does not necessitate it arriving at the cortex before red-green information.
523

latency of CIECAM02-a expression (red) and CIECAM02-A
expression (blue), relative to the visual stimulus (ms)

524
525 **Fig 5. Expression distributions for CIECAM02-a and CIECAM02-A superimposed on a**
526 **single plot.** Figs 3A (**CIECAM02-a, red**) and 3B (**CIECAM02-A, blue**) are superimposed
527 to show CIECAM02-A lagging CIECAM02-a by 40 ms. As in Fig 3, the peaks for both
528 models' significant expression are marked X (at 35 ms, CIECAMO2-a) and Y (75 ms,
529 CIECAMO2-A).

530 If this latency mismatch is indeed a result of delay caused by retinal physiology, what
531 repercussions might this have on downstream visual processing? The output of colour
532 opponency processing is thought to feed into processes such as edge and relief
533 detection (Hansen and Gegenfurtner, 2009; Kingdom, 2003), and a mismatch in
534 latency must affect such processes, at least for rapidly moving stimuli. Either the two
535 channels are integrated with the delay still present, or the chromatic representation
536 would need to be delayed in order to correct the difference. If the latter, we might
537 expect to observe a secondary spike of entrainment to CIECAM02-a at 75 ms,
538 demonstrating that CIECAM02-a had become re-synchronised. But such an
539 observation would not be necessary for such an account to hold – both CIECAM02-a
540 and CIECAM02-A may have further transforms applied to them before being
541 resynchronised. Given that the present study is not designed to be sensitive to such
542 models, it suggests a need for future research.

543 Overall, the results of this study support the view that visual information from the L-
544 and M-cones integrate into a single red-green opponent channel in the manner
545 modelled by CIECAM02-a, which exhibits entrainment at 35 ms delay in the occipital
546 lobe region of the cortex. In parallel to this, visual information from the L- and M-
547 cones combine into an achromatic channel in the manner modelled by CIECAM02-A,
548 exhibiting entrainment at 75 ms delay in the occipital lobe region (Fig 6.)

549

550
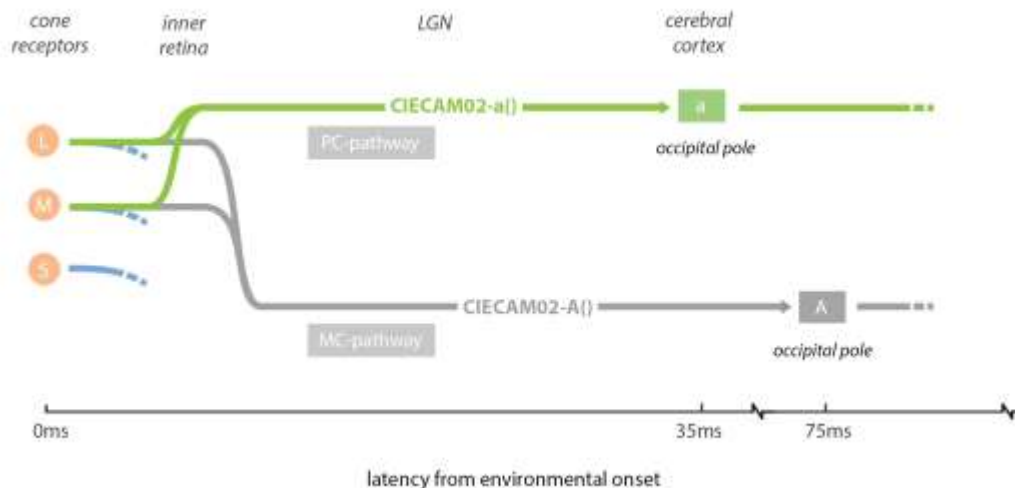
**Fig 6. Implied pathway of red-green colour opponent and achromatic response
information.** The interpretation of the pathways suggested by the findings of this study.
Information from the visual field enters the nervous system as L, M and S values, from which
L and M is combined into the CIECAM02-a model component, exhibiting entrainment at 35
ms in the occipital lobe region of the cortex. In parallel, L- and M-cone information is
combined into the CIECAM02-A model component, exhibiting in entrainment at 75 ms in the
occipital lobe region of the cortex. In the model, both components also receive minor inputs
from S cones, but these contributions have been left out for clarity. The incomplete blue
pathways leaving L, M, S are the assumed inputs to the cyan-yellow KC-pathway (not tested
in this study).

It should be emphasized that this characterisation — based on plausibilities of the
models tested in this study — must be seen as a simplification of the full picture of
chromatic and achromatic transforms taking place between the retina and V1. While
single-cell recordings in macaque and rhesus monkeys confirm that the retina, LGN
and V1 all contain cells which are selective to chromatic or achromatic information
(e.g. retina: Gouras, 1968; De Monasterio and Gouras, 1975; LGN: Derrington et al,
1984; Levitt et al, 2001; V1: Johnson et al, 2001; Conway, 2001), such cells, both in
the retina and LGN, have also been shown to carry other properties of the stimulus,
for example the ratio of stimulus's centre/surround in the cells' receptive field (De
Monasterio and Schein, 1980; Wiesel and Hubel, 1966). Indeed, it appears colour-
opponency cells are tuned to a range of properties: in V1 these include spatial
frequency, orientation and more complex hue spaces (Leventhal, et al, 1995; Johnson
et al, 2008; Wachtler et al, 2003), as well as cells that respond to both luminance and
colour (Johnson et al, 2001; Johnson et al, 2004; Thorell, et al 1984), and there are
indications of tuning to properties such as orientation as early as LGN MC- and PC-
cells (Xu et al, 2000). This indicates a picture where the steps in visual processing
leading to colour perception are complex combination of transforms that take place
over the retina-LGN-V1 pathway.

The findings reported in this study open a number of avenues for further work. First, repeating the above study using electroretinography may help identify the latency at which various chromatic components leave the retina; this would, in turn, narrow down the latency window between which these components travelled from the retina to V1. Testing cortical entrainment to the cyan-yellow colour opponent response (as estimated by CIECAM02-b) is a second reasonable extension to this work; the KC-pathway is less studied that the pathways tested above and its delay in latency relative to the PC- and MC-pathways is unknown. It would also be beneficial to test further components of the CIECAM02 model beyond the three central colour pathways, as well as rival colour opponency and luminance models (e.g. Kunkel and Reinhard, 2009). The CIECAM02 model does not, for instance, take into account historical values of visual input, and so does not model the fact that red-green entrainment is reported to break down for higher frequencies (Ives, 1912).

4.1 Overview

The results from this study suggest that the CIECAM02-a transform of the visual field occurs before a latency of 35 ms, with entrainment to the output of this transform occurring at 35 ms latency bilaterally in occipital lobe regions. In parallel to this, the CIECAM02-A transform also takes place, with entrainment occurring at 75 ms, also in the occipital lobe regions. By comparison, no entrainment was found to the relatively physiologically naive CIELAB-L and CIELAB-A components. The locations of the significant entrainment are only approximate due to the inherent error in source estimation of EMEG data and more work is needed in improving the accuracy of these reconstructions in order to improve the certainty of these locations.

5. Data statement

The data used in this study (including stimuli, EMEG recordings and pre-processed data) can be found at https://kymata.org/datasets, available under a CCBY licence.

6. Acknowledgements

619

620

7. References

622

623 Brainard, D. H. (1997) The Psychophysics Toolbox, *Spatial Vision,* 10:433-436 doi:
624 10.1163/156856897X00357

625 Bone, R.A. and Sparrock, J.M.B. (1971). Comparison of macular pigment densities in
626 the human eye. *Vis. Res.*11: 1057-1064. doi: 10.1016/0042-6989(71)90112-X

627 Cheng, M., Gao, X., Gao, S., Xu, D. (2001) Multiple color stimulus induced steady
628 state visual evoked potentials. *Proc. IEEE EMBS*, 2:1012–1014. doi:
629 10.1109/IEMBS.2001.1020359

630 Conway B.R. (2001) Spatial structure of cone inputs to color cells in alert macaque
631 primary visual cortex (V-1). *J Neurosci*. 21: 2768–83.

632 Conway, B. R., Chatterjee, S., Field, G. D., Horwitz, G. D., Johnson, E. N., Koida, K.,
633 and Mancuso, K. (2010) Advances in Color Science: From Retina to Behavior. *J.*
634 *Neurosci*. 30:14955–14963 doi: 10.1523/JNEUROSCI.4348-10.2010

635 Dacey, D. M., Lee, B.B., Stafford, D.M., Smith, V.C., Pokorny, J. (1996) Horizontal
636 cells of the primate retina: cone specificity without cone opponency. *Science*. 271:
637 656–8 doi: 10.1126/science.271.5249.656

638 Davis, M., Sigal, R. and Weyuker, E. J. (1994). *Computability, complexity, and*
639 *languages: fundamentals of theoretical computer science*. Burlington, MA: Morgan
640 Kaufmann Pub.

641 De Monasterio, F. M. & Gouras, P. (1975). Functional properties of ganglion cells of
642 the rhesus monkey retina. J Physiol. 251, 167-195.

643 De Monasterio, F.M. and Schein, S.J. (1980) Protan-Like Spectral Sensitivity of
644 Foveal Y Ganglion Cells of the Retina of Macaque Monkeys. *J. Physiol.* 299: 385-
645 396

646 Derrington, M., Krauskopf, J., and Lennie, P. (1984) Chromatic Mechanisms in
647 Lateral Geniculate Nucleus of Macaque. *J Physiol*. 357: 241-265 doi:
648 10.1113/jphysiol.1984.sp01549

649 Engel, S., Zhang, X and Wandell, B. (1997) Colour tuning in human visual cortex
650 measured with functional magnetic resonance imaging. *Nature* 388: 68-71 doi:
651 10.1038/40398

652 Fairchild, M. D. (2013) *Color Appearance Models*, Third Edition. Oxford, England:
653 Wiley

654 Fischl, B., Sereno, M. I., Tootell, R.B., Dale, A.M. (1999) High-resolution inter-
655 subject averaging and a coordinate system for the cortical surface. *Hum Brain Mapp.*
656 8:272-284.

657 Gouras, P. (1968). Identification of cone mechanisms in monkey ganglion cells. J of
658 Physiol 199, 533-547.

659 Grave de Peralta-Menendez, R., Gonzalez-Andino, S. L., and Lutkenhoner, B. (1996).
660 Figures of merit to compare linear distributed inverse solutions. *Brain. Topogr.*
661 9:117–124. doi: 10.1007/BF01200711

662 Grave de Peralta-Menendez, R., and Gonzalez-Andino, S. L. (1998). A critical
663 analysis of linear inverse solutions to the neuroelectromagnetic inverse problem.
664 *IEEE Trans. Biomed.* Eng. 45, 440–8. doi: 10.1109/10.664200

665 Hadjikhani, N., Liu, A. K., Dale, A. M., Cavanagh, P., & Tootell, R. B. (1998).
666 Retinotopy and color sensitivity in human visual cortical area V8. Nature
667 Neuroscience, 1, 235–241

668 Hämäläinen, M.S., Ilmoniemi, R.J. (1994) Interpreting magnetic fields of the brain:
669 minimum norm estimates. *Med Biol Eng Comput.* 32:35-42. doi:
670 10.1007/BF02512476

671 Hansen, T., and Gegenfurtner, K.R. (2009) Independence of color and luminance
672 edges in natural scenes. *Vis Neurosci.* 26:35–49. doi:10.1017/S0952523808080796

673 Hauk, O., Wakeman D. G., and Henson, R. (2011). Comparison of noise-normalized
674 minimum norm estimates for MEG analysis using multiple resolution metrics.
675 *NeuroImage* 54, 1966-1974. doi: 10.1016/j.neuroimage.2010.09.053

676 Hering, E. (1878) *Zur Lehre vom Lichtsinn* Berlin: Springer

677 Herrmann, C.S. (2001). Human EEG responses to 1-100 Hz flicker: resonance
678 phenomena in visual cortex and their potential correlation to cognitive phenomena.
679 *Exp. Brain Res.* 137: 346–353. doi:10.1007/s002210100682

680 Hunt, R. W. G and Pointer, M. R. (1985) A colour appearance transform for the 1931
681 standard colorimetric observer. *Col Res Appl,* 10, 165-179 doi:
682 10.1002/col.5080100306

683 ISO/CIE (1999) ISO 10526:1999/CIE S005/E-1998: Standard Illuminants for
684 Colorimetry. Vienna, Austria: ISO/CIE

685 ISO (2007) 11664-1:2007 Colorimetry -- Part 1: CIE standard colorimetric observers
686 International Organization for Standardization, Geneva, Switzerland.

687 Ives, H. E. (1912). Studies in the photometry of lights of different colours. I. Spectral
688 luminosity curves obtained by the equality of brightness photometer and flicker
689 photometer under similar conditions. *Phil. Mag. Ser.* 6:149–188. doi:
690 10.1080/14786440708637317

691 Johnson, E. N., Hawken M. J. and Shapley R. (2001) The spatial transformation of
692 color in the primary visual cortex of the macaque monkey. *Nat. Neurosci.* 4, 409–
693 416 doi:10.1038/86061

694 Johnson, E. N., Hawken, M. J., Shapley, R. (2004) Cone inputs in macaque primary
695 visual cortex. *J Neurophysiol.* 91: 2501–14. doi:10.1152/jn.01043.2003.

696 Johnson, E.N., Hawken, M.J., Shapley, R. (2008) The orientation selectivity of color-
697 responsive neurons in macaque V1. *J Neurosci.* 28: 8096–106. doi:
698 10.1523/JNEUROSCI.1404-08.2008

699 Johnson, E.N., Mullen, K.T. (2016) Color in the Cortex. In: Kremers J., Baraas R.,
700 Marshall N. (eds) *Human Color Vision*. Springer: Cham: doi: 10.1007/978-3-319-
701 44978-4_7

702 Judd, D. B., (1951) Basic correlates of the visual stimulus *Handbook of Experimental*
703 *Psychology,* Stevens, S. S. (Ed), pp. 811-867. Oxford, England: Wiley

704 Kingdom, F.A. (2003) Color brings relief to human vision. *Nat Neurosci.* 6: 641–4.
705 doi:10.1038/nn1060

706 Kleiner, M., Brainard, D., Pelli, D. (2007) What's new in Psychtoolbox-3? *Perception*
707 36:14, doi:10.1177/03010066070360S101

708 Kommanapalli, D, Murray, I. J., Kremers, J., Parry, N. R. A. and McKeefry, D. J.
709 (2014) Temporal characteristics of L- and M-cone isolating steady-state
710 electroretinograms *J. Opt. Soc. Am.* A 31: A113-A120 doi:
711 10.1364/JOSAA.31.00A113

712 Kremers, J. and Link, B. (2008) Electroretinographic responses that may reflect
713 activity of parvo- and magnocellular post-receptoral visual pathways. *J Vis.* 8:1–14.
714 doi: 10.1167/8.15.11

715 Kremers, J., Rodrigues, A.R., Silveira, L.C.L., da Silva-Filho, M. (2010) Flicker
716 ERGs representing chromaticity and luminance signals. *Invest Ophthalmol Vis Sci.*
717 51:577–87 doi:10.1167/iovs.09-3899

718 Kunkel, T., Reinhard, E. (2009) A neurophysiology-inspired steady-state color
719 appearance model. *J Opt Soc Am A* 26:776-82. doi: 10.1364/JOSAA.26.000776

720 Kwong, K. K., Belliveau, J. W., Chesler, D. A., Goldberg, I. E., Weisskoff, R. M.,
721 Poncelet, B. P., et al. (1992). Dynamic magnetic resonance imaging of human brain
722 activity during primary sensory stimulation. *PNAS*, 89: 5675–5679 doi:
723 10.1073/pnas.89.12.5675

724 The Kymata Atlas; Cambridge University (2016) https://kymata.org/

725 Lalor, E.C., Pearlmutter, B.A., Reilly, R.B., McDarby, G., and Foxe, J.J. (2006) The
726 VESPA: a method for the rapid estimation of a visual evoked potential. *Neuroimage*
727 32:1549–1561. doi: 10.1016/j.neuroimage.2006.05.054

728 Li, C., Luo, M.R., Rigg, B., Hunt, R.W.G. (2002) CMC2000 Chromatic Adaptation
729 Transform: CMCCAT2000. *Col Res Appl*. 27:49-58 doi: 10.1002/col.10005

730 Lee, B.B., Silveira, L.C.L. (2016) Cone Opponency: An Efficient Way of
731 Transmitting Chromatic Information. In: Kremers J., Baraas R., Marshall N. (eds)
732 *Human Color Vision*. Springer: Cham. doi: 10.1007/978-3-319-44978-4_4

733 Leventhal, A.G., Thompson, K.G., Liu, D., Zhou, Y., Ault, S.J. (1995) Concomitant
734 sensitivity to orientation, direction, and color of cells in layers 2, 3, and 4 of monkey
735 striate cortex. *J Neurosci*. 15: 1808–18.

736 Levitt, J. B., Schumer, R. A., Sherman, S. M., Spear, P.D., and Movshon J. A. (2001)
737 Visual Response Properties of Neurons in the LGN of Normally Reared and Visually
738 Deprived Macaque Monkeys. *J Neurophys*. 85: 2111-2129. doi:
739 10.1152/jn.2001.85.5.211

740 Luo, M. R., and Hunt, R. W. G. (1998). Testing colour appearance models using
741 corresponding-colour and magnitude-estimation datasets. *Color Research &*
742 *Application 23*, 3, 147– 153. doi: 10.1002/(SICI)1520-6378(199806)23:3<147::AID-
743 COL6>3.0.CO;2-Q

744 Macleod, D. I. and Boynton, R. M. (1978) Chromaticity diagram showing cone
745 excitation by stimuli of equal luminance. *J Opt Soc Am*. 69: 1183-1186 doi:
746 10.1364/JOSA.69.001183

747 McKeefry, D.J. and Zeki, S. (1997) The position and topography of the human colour
748 centre as revealed by functional magnetic resonance imaging. *Brain*, 120**,** 2229–2242

749 Moroney, N., Fairchild, M. D., Hunt, R. W., Li, C., Luo, M. R., and Newman, T.
750 (2002). The CIECAM02 color appearance model. *10th Color and Imaging*
751 *Conference Final Program and Proceedings* (pp. 23-27). Society for Imaging Science
752 and Technology.

753 Nishifuji, S., Ohkado, H., Tanaka, S., 2006. Characteristics of alpha wave response to
754 flicker stimuli with color alternation. *Electronics and Communications in Japan, Part*
755 *3* (Translated from *Denshi Joho Tsushin Gakkai Ronbunshi*, 2005.) 89: 480-489.
756 doi: 10.1002/ecjc.20204

757 Ogawa, S., Tank, D., Menon, R., Ellermann, J., Kim, S., Merkle, H., et al (1992)
758 Intrinsic signal changes accompanying sensory stimulation: Functional brain mapping
759 with magnetic resonance imaging. *PNAS* 89:591–5955. Doi: 10.1073/pnas.89.13.5951

760 Parry, N. R. A., Murray, I. J., Panorgias, A., Mckeefry, D. J., Lee, B. B., Kremers, J.
761 (2012) Simultaneous chromatic and luminance human electroretinogram responses. *J*
762 *Physiol*. 150: 3141–3154 doi: 10.1113/jphysiol.2011.226951

763 Pelli, D. G. (1997) The VideoToolbox software for visual psychophysics:
764 Transforming numbers into movies, *Spat. Vis.* 10, 437-442. doi:
765 10.1163/156856897X00366

766 Regan, D. (1966). Some characteristics of average steady-state and transient
767 responses evoked by modulated light. *Electroencephalogr. Clin. Neurophysiol.* 20,
768 238–248. doi: 10.1016/0013-4694(66)90088-5

769 Ripamonti, C., Woo, W. L., Crowther, E., and Stockman, A. (2009) The S-cone
770 contribution to luminance depends on the M- and L-cone adaptation levels: Silent
771 surrounds? *J. Vision*, 9:10, 1–16, doi:10.1167/9.3.10.

772 Schmahmann, J. D., Doyon, J., Toga, A. W., Petrides, M., and Evans, A. C. (2000).
773 *MRI Atlas of the Human Cerebellum.* San Diego, CA: *Academic Press*.

774 Shapley, R., Hawken M. J. (2011) Color in the Cortex: single- and double-opponent
775 cells. *Vis. Res.* 51: 701–717 doi:10.1016/j.visres.2011.02.012

776 Smith, V.C., Lee, B. B., Pokorny, J., P. R. Martin, and A. Valberg, A. (1992)
777 Responses of macaque ganglion-cells to the relative phase of heterochromatically
778 modulated lights, *J. Physiol.* 458, 191-221. doi: 10.1113/jphysiol.1992.sp019413

779 Stockman, A., and Sharpe, L. T. (2000) Spectral sensitivities of the middle- and long-
780 wavelength sensitive cones derived from measurements in observers of known
781 genotype. *Vis. Res.*, 40, 1711-1737. doi: 10.1016/S0042-6989(00)00021-3

782 Stockman, A., Sharpe, L. T., and Fach, C. C. (1999) The spectral sensitivity of the
783 human short-wavelength cones. *Vis. Res.*, 39, 2901-2927. doi: 10.1016/S0042-
784 6989(98)00225-9

785 Taulu, S., Simola, J., Kajola, M. (2005) Applications of the signal space separation
786 method. IEEE T Signal Proces. 53:3359-3372. doi: 10.1109/TSP.2005.853302

787 Thorell, L.G., De Valois, R.L., Albrecht, D.G. (1984) Spatial mapping of monkey V1
788 cells with pure color and luminance stimuli. *Vision Res.* 24:751–69 doi:
789 10.1016/0042-6989(84)90216-5

790 Thwaites, A., Nimmo-Smith, I., Fonteneau, E., Patterson, R.D., Buttery, P., Marslen-
791 Wilson, W.D. (2015) Tracking cortical entrainment in neural activity: auditory
792 processes in human temporal cortex. *Front Comp Neurosci*.1-14 doi:
793 10.3389/fncom.2015.00005

794 Thwaites, A., Schlittenlacher, J., Nimmo-Smith, I., Marslen-Wilson W.D., Moore,
795 B.C.J. (2017) Tonotopic representation of loudness in the human cortex. *Hear. Res.*
796 344: 244-254 doi:10.1016/j.heares.2016.11.015

797 Thwaites, A., Glasberg, B.R., Nimmo-Smith, I., Marslen-Wilson W.D., Moore, B.C.J.
798 (2016) Representation of Instantaneous and Short-Term Loudness in the Human
799 Cortex. *Front. Neurosci.* 10: 183 doi:10.3389/fnins.2016.00183

800 Thwaites, A., Nimmo-Smith, I., Wieser, E., Soltan, A., Marslen-Wilson, W. D.
801 (2016b) *Measurement datasets 1-3.01 for the Kymata Atlas* [Dataset]. doi:
802 10.17863/CAM.1660

803 VanRullen, R. Macdonald, J.S.P. (2012) Perceptual Echoes at 10 Hz in the Human
804 Brain. *Cur Biol* 22:995–999 doi: 10.1016/j.cub.2012.03.050

805   Wachtler, T., Sejnowski, T.J., Albright, T.D. (2003) Representation of color stimuli in
806   awake macaque primary visual cortex. *Neuron*. 37: 681–91 doi: 10.1016/S0896-
807   6273(03)00035-7

808   Wade, A., Augath, M., Logothetis, N., Wandell, B. (2008). fMRI measurements of
809   color in macaque and human. *J Vis*, 8: 1–19, doi: 10.1167/8.10.6

810   Walraven, P. L., and Leebeek, H. J. (1964) Phase shift of alternating coloured stimuli
811   *Doc. Ophthalmol.* 18, 56–71. doi: 10.1007/BF00160563

812   Wandell, B. A. (1995) *Foundations of Vision*, Sunderland, MA: Sinauer Associates
813   Inc.

814   Wandell, B. A., Winawer, J. (2011) Imaging retinotopic maps in the human brain. *Vis
815   Res* 51:718–737 doi: 10.1016/j.visres.2010.08.004

816   Wiesel T, Hubel DH. (1966) Spatial and chromatic interactions in the lateral
817   geniculate body of the rhesus monkey. *J Neurophysiol.* 29:1115–56 doi:
818   10.1152/jn.1966.29.6.1115

819   Xu, X., Ichida, J., Shostak, Y., Bonds, A., and Casagrande, V. (2002). Are primate
820   lateral geniculate nucleus (LGN) cells really sensitive to orientation or direction? *Vis.
821   Neurosci.*, 19: 97-108. doi:10.1017/S0952523802191097

822

823